Journal of Applied Polymer Science

Improved Thermostability and Interfacial Matching of Nanoclay Filler and Ethylene Vinyl Alcohol Matrix by Silane-Modification

Björn Geyer,[1] Stefan Röhner,[1] Günter Lorenz,[1,2] Andreas Kandelbauer[1,2]

[1]Reutlingen Research Institute (RRI), Reutlingen University, Alteburgstrasse 150 72762 Reutlingen, Germany

[2]School of Applied Chemistry, Reutlingen University, Alteburgstrasse 150 72762 Reutlingen, Germany

Correspondence to: A. Kandelbauer (E-mail: andreas.kandelbauer@reutlingen-university.de)

ABSTRACT: The interfacial compatibility between polymers and nanoclay fillers as well as the thermostability of both components are important characteristics for processing them into polymer composites. While the polymer component is often grafted using common polymerization reactions, the nanoclay component is usually surface modified by surfactant treatment to improve compatibility. In the present study, the polymer ethylene vinyl alcohol and a nanoclay filler based on natural bentonite are both surface modified by different silanes, 3-glycidoxypropyltrimethoxysilane and methacryloxymethyltrimethoxysilane and their interfacial properties are investigated by inverse gas chromatography. The silane-modified samples had improved interfacial properties as reflected by a significant increase in dispersive and specific surface energies. Lewis acidities were determined using chloroform and 1,4-dioxane as polar probes and showed a good match between polymer and nanofiller interfaces. Lewis acidity was generally lower after silane-modification. Silanization yielded increased thermal stability of the treated samples. Thus, silanization led to improved compatibility and enhanced thermal stability which facilitates further processing. © 2014 Wiley Periodicals, Inc. J. Appl. Polym. Sci. **2015**, *132*, 41227.

KEYWORDS: clay; compatibilization; grafting; polyolefins; surfaces and interfaces

Received 19 March 2014; accepted 28 June 2014

DOI: 10.1002/app.41227

INTRODUCTION

Adjustment and enhancement of the heat-resistance and the interfacial properties of polymers and nanoclays are important prerequisites for providing processability of the components for advanced polymer nanocomposite materials.[1–13]

Compatibilization of nanoclay is generally achieved by surfactant treatment, where an ionic bonding of organic surfactants to the silicate surface is established.[14–17] On the other hand, surface modification of polymers is often accomplished by the grafting of polymers using common polymerization reactions.[18–20] Silanization of either the polymer or the nanoclay filler has also been described in the literature for this purpose.[21–24] However, to the best of our knowledge, the simultaneous use of silane coupling agents for the surface treatment of both polymers and nanoclays have so far not yet been described in the literature. Such silane modification should yield ideal surface compatibility since the functional groups introduced into both components display a high degree of chemical similarity. Compatibility of two components in a mixture generally is determined by their relative surface energies. Similar values for the surface energies of two materials usually lead to improved wetting and adhesion behavior and, in turn, improved compatibility.[25] Surface energies are typically determined via contact angle measurements or inverse gas chromatography (IGC). Although there are numerous reports dealing with the interfacial properties of either matrix systems or fillers intended for blending,[3,9,13,18,26–28] no combined studies exist that focus on the quantitative characterization of the interfacial properties of ethylene vinyl alcohol and nanoclays where the interfacial properties of both components are modified in order to improve and adjust the intermolecular interaction forces.

The present contribution deals with the preparation of silane-modified EVOH and silane-modified nanoclay to adjust the surface energies for improved compatibility and thermostability of the two modified components. All samples were characterized by IGC and contact angle measurements (CA) to quantify the interfacial energies and to determine the Lewis acid-base properties of modified EVOH and modified nanoclay. Furthermore, thermostability of these materials was investigated by thermogravimetric (TGA) measurements.

EXPERIMENTAL

Chemicals

Ethylene vinyl acetate (EVA, Levapren®) with a vinyl acetate content of 70.5% obtained from Bayer AG (Leverkusen, Germany) was used for the synthesis of ethylene vinyl alcohol

Table I. Stoichiometry and Reaction Conditions for Modification of EVOH with MAOM-TMOS and GOP-TMOS

Sample	Mass EVOH (g)	Silane	Volume silane (mL)	Amount of silane (mmol)	VOH (mmol)	pH	t_R (h)
ES1	3.3	MAOM-TMOS	2.6	14	41	4.6	6
ES2	3.3	MAOM-TMOS	2.6	14	41	4.6	48
ES3	3.3	MAOM-TMOS	2.6	14	41	7.0	6
ES4	3.3	MAOM-TMOS	2.6	14	41	7.0	48
ES5	3.3	GOP-TMOS	3.1	14	41	4.6	6
ES6	3.3	GOP-TMOS	3.1	14	41	4.6	48
ES7	3.3	GOP-TMOS	3.1	14	41	7.0	6
ES8	3.3	GOP-TMOS	3.1	14	41	7.0	48

VOH: amount of vinyl alcohol in ethylene vinyl alcohol; t_R: reaction time.

(EVOH). Grafting reagents procured from Wacker Chemie AG (Munich, Germany) were 3-glycidoxypropyltrimethoxysilane (GOP-TMOS, tradename Geniosil® GF80) and methacryloxymethyltrimethoxysilane (MAOM-TMOS, tradename Geniosil® XL33). As a natural bentonite (NBt) the organically modified nanoclay Nanofil® 5 supplied by Rockwood Clay Additives GmbH (Moosburg, Germany) was used for all experiments. Dimethylformamide (DMF) supplied by Th. Geyer GmbH (Renningen, Germany) was used as swelling agent for suitable processing of the nanoclay. Surface properties of modified EVOH and nanoclay were characterized by IGC using *n*-hexane, *n*-heptane, *n*-octane, and *n*-nonane as non-polar probes. Polar probe molecules were chloroform and 1,4-dioxane. Methane was used as the non-interacting probe. For contact angle measurements water and *n*-decane were used. All probes were of analytical grade and were purchased from Th. Geyer (Renningen, Germany).

Methods

Synthesis and Modification of EVOH with Different Silanes. EVOH was synthesized according to a procedure described in detail elsewhere.[29] Ethylene vinyl acetate (EVA) was dissolved in toluene and a stoichiometric amount of ethanolic potassium hydroxide solution was added. The mixture was heated to 70°C for 3 h. EVOH was precipitated upon addition of diluted hydrochloric acid. EVOH was washed with a mixture of water/acetone, filtered off and dried under vacuum at 80°C.

For modification with silanes, aliquots of EVOH were dissolved in DMF under inert gas atmosphere (N_2). Stoichiometric amounts of each silane, GOP-TMOS, or MAOM-TMOS were added and stirred at 60°C for defined reaction times. Prior to EVOH modification, the silanes were activated for 10 min in an ethanol-water mixture (1 : 1, v/v). In the experimental design the factors "reaction time" for the modification and "pH-value" at which silane activation and modification was performed were varied. The reaction mixtures were stirred for either 6 h or 48 h at a pH value of either 4.6 or 7.0 (Table I). Subsequently, the crude products were precipitated from solution with brine, filtered off, and washed with water. The obtained samples were dried under vacuum at 80°C for 24 h.

Modification of Nanoclay with Different Silanes. The nanoclay NBt was modified by two different silanes MAOM-TMOS and GOP-TMOS as follows. Initially, 1 g of the nanoclay was pretreated for 1 h with a Sonotrode HD 2200 VS 70 T (Bandelin electronic, Berlin, Germany) in DMF to improve swelling properties. Subsequently, each suspension of nanoclay was treated with either 40, 70, or 100 mmol of the respective silane. The samples were stirred for 16 h, then washed with ethanol and water, filtered off, and dried under vacuum at 80°C overnight.

Structural Characterization of Silane-Modified EVOH and Silane-Modified Nanoclay. Structural characterization of silane-modified EVOH and silane-modified nanoclay was performed by ^{1}H and ^{29}Si nuclear magnetic resonance spectroscopy and infrared spectroscopy.

^{1}H-NMR-spectra of silane-modified EVOH were recorded on a Bruker AC 250 NMR spectrometer (University of Tübingen, Germany). Magnetic field strength was 5.85 T (250.10 MHz for ^{1}H) at 27°C, ^{1}H 90° pulse length was 9.6 µs and spectral width was 4000 Hz. Samples were dissolved in deuterated dimethyl sulfoxide (DMSO-d6).

^{29}Si-Cross polarization/magic angle spinning (CP/MAS) solid state nmr spectra of the samples were recorded on a Bruker ASX 300 (^{29}Si) (University of Tübingen, Germany). Magnetic field strength was 7.05 T (59.62 MHz for ^{29}Si) at room temperature. The proton 90° pulse length was 6.2 µs (^{29}Si). Spectral width was 17,921.15 Hz (^{29}Si). Magic angle spinning was performed at 4 kHz (^{29}Si).

Infrared spectroscopy was used to obtain a general overview of the structure of silane-modified EVOH and silane-modified nanoclay. KBr-pellets were prepared from unmodified and modified samples. Infrared spectra were recorded in transmission before and after modification using a Spectrum One (Perkin Elmer LAS GmbH, Rodgau-Jügisheim, Germany). Each sample was measured within a wavenumber range between 4000 cm^{-1} and 650 cm^{-1}. Each spectrum was an average of 16 single wavelength scans.

Additionally, to investigate the effect of silane-modification on the inter-layer distance of nanoclay samples X-ray diffraction measurements (XRD) were conducted. X-ray diffraction patterns of powdery samples were recorded using a Siemens D5005 diffractometer (Cu Kα 1.54 Å) equipped with a secondary monochromator operating at 40 kV and 40 mA. Nitrogen

adsorption measurements were performed on a Quantachrome Autosorb 6. The specific surface areas of nanoclay samples were calculated according to the Brunauer-Emmett-Teller (BET) method. Total pore volumes and pore size distributions of nanoclay samples were calculated with the Barrett–Joyner–Halenda (BJH) method.

Characterization of Surface Properties. ***Inverse gas chromatography.*** Dispersive surface energy and specific desorption energy of silane-modified EVOH and silane-modified nanoclay were determined by IGC. The Gas Chromatograph Agilent 6890 Series was equipped with flame ionization detector (FID) and Chemstation control software version 1.5 from Porotec GmbH (Hofheim/Ts., Germany). Physicochemical data was evaluated with IGC analysis software version 1.1 (Surface measurements Systems, Alperton Middlesex, London, UK). The carrier gas was helium with a flow rate of 20 $cm^3\ min^{-1}$.

Prior to surface characterization samples were ground and sieved [60 mesh (US), 250 μm]. To avoid column blocking each sample (0.1 g) was mixed with inert glass beads (size 0.25–0.5 mm). Prepared samples were packed in silanized glass columns (length 0.3 m) with internal diameter of 3 mm. To prevent spillage of sample mass, columns were plugged at both ends with silanized glass wool. Samples were conditioned at 35°C (308 K) and 0 % relative humidity for 12 h under helium gas flow of 20 $cm^3\ min^{-1}$. Injection of *n*-alkanes was made at a partial pressure of 0.05 p/p_0. Dead time volume determination was made by the injection of methane gas at a partial pressure of 0.01 p/p_0. Samples were measured twice. Injection of a series of *n*-alkanes was performed to calculate dispersive surface energy γ_S^D using the approach of Schultz et al. which is briefly summarized in the following section.[30–32]

Starting with the experimental determination of the retention time of a non-polar probe molecule (t_r) and a non-interacting probe (t_0) at certain carrier gas flow F the net retention volume V_N is calculated according to eq. (1) taking into account the James–Martin correction factor D [eq. (2)] for gas compressibility.

$$V_N = F \cdot D \cdot (t_r - t_0) \tag{1}$$

$$D = \frac{3 \cdot \left[\left(\frac{p_i}{p_0}\right)^2 - 1\right]}{2 \cdot \left[\left(\frac{p_i}{p_0}\right)^3 - 1\right]} \tag{2}$$

Under the assumption of Dorris and Gray[33] the desorption energy ΔG can be approximated by the product of Avogadro's number $\mathcal{N}$, the work of adhesion W to the solid surface and cross sectional area a of the probe molecule adsorbed [eq. (3)].

$$\Delta G = \mathcal{N} \cdot a \cdot W \tag{3}$$

Using *n*-alkane probes, Fowkes related the work of adhesion W to the dispersive surface energy γ_S^D of the solid under investigation and to the dispersive surface energy γ_L^D of liquid probes, represented in eq. (4).[34]

$$W = 2\sqrt{\gamma_S^D \gamma_L^D} \tag{4}$$

By the combination of eqs. (3) and (4), the desorption energy ΔG can be expressed as follows:

$$\Delta G = \mathcal{N} \cdot a \cdot 2\sqrt{\gamma_S^D \gamma_L^D} \tag{5}$$

On the other hand ΔG can be expressed as a function of the net retention volume V_N by thermodynamic considerations at infinite dilution as usually applied to IGC [eq. (6)], where C is a constant depending on the reference state.[32]

$$\Delta G = RT \cdot \ln V_N + C \tag{6}$$

Rearrangement of eqs. (5) and (6) leads to eq. (7), from which the dispersive surface energy γ_S^D of a solid sample can be calculated from the slope of the *n*-alkane line (reference line) from plotting $RT \ln V_N$ against $a\left(\gamma_L^D\right)^{\frac{1}{2}}$.[30,32]

$$RT \ln V_N = 2\mathcal{N}\left(\gamma_S^D\right)^{\frac{1}{2}}\ a\ \left(\gamma_L^D\right)^{\frac{1}{2}} + C \tag{7}$$

In addition the injection of polar probe molecules enables characterization of Lewis acid-base properties. For this purpose the desorption energy ΔG is calculated as sum of the dispersive desorption energy ΔG^D and the specific desorption energy ΔG^{sp}. These energies (ΔG^D, ΔG^{sp}) are substituted by the relationship of Dorris and Gray [eq. (3)] yielding eq. (8), where W^D, W^{sp} are the dispersive and specific work of adhesion of an adsorbed probe molecule.[35]

$$\Delta G = \Delta G^D + \Delta G^{sp} = \mathcal{N} \cdot a \cdot W^D + \mathcal{N} \cdot a \cdot W^{sp} \tag{8}$$

Furthermore, ΔG^D can be expressed in dependence of a reference net retention volume V_N^{ref} [eq. (9)]. V_N^{ref} is derived from the *n*-alkane reference line at $a\left(\gamma_L^D\right)^{\frac{1}{2}}$ of the corresponding polar probe molecule.

$$\Delta G^D = \mathcal{N} \cdot a \cdot W^D = RT \ln V_N^{ref} \tag{9}$$

With the desorption energy expressed in terms of a net retention volume [eq. (6)], eq. (8) is transformed by combination of eqs. (6) and (9) (eq. (10)). Rearrangement of eq. (10) leads to the expression for the specific desorption energy ΔG^{sp} [eq. (11)]:[30,32,35]

$$RT \ln V_N = RT \ln V_N^{ref} + \mathcal{N} \cdot a \cdot W^{sp} = RT \ln V_N^{ref} + \Delta G^{sp} \tag{10}$$

$$\Delta G^{sp} = RT \ln V_N - RT \ln V_N^{ref} \tag{11}$$

Lewis acid–base properties of silane treated samples were calculated as the ratio of the specific desorption energies ΔG^{sp} from 1,4-dioxane and chloroform. This ratio indicates an acidic ($\frac{\Delta G^{sp}(Dioxane)}{\Delta G^{sp}(Chloroform)} \geq 1.1$) or basic character ($\frac{\Delta G^{sp}(Dioxane)}{\Delta G^{sp}(Chloroform)} \leq 0.9$) of the solid surface.[36]

Characteristic physicochemical parameters of used probe molecules required for calculation of surface properties are listed in Table II.

Table II. Characteristic Parameters of Used Probe Molecules [31,32,37,38]

Probe	$a[Å^2]$	$\gamma_L^D[mJ \cdot m^{-2}]$	$\frac{a\sqrt{\gamma_L^D}}{[Å^2\sqrt{mJ \cdot m^{-2}}]}$
n-Hexane	51.5	18.4	220.9
n-Heptane	57.3	20.3	258.2
n-Octane	63.0	21.3	290.8
n-Nonane	69.0	22.7	328.7
Chloroform	44.0	25.0	220.0
1,4-Dioxane	31.4	33.2	180.9

Cross-sectional area of a probe molecule in $Å^2$.
γ_L^D: Dispersive surface energy of liquid probe in mJ m^{-2}.

Contact angle measurements. Additionally, the surface properties were characterized by measuring the contact angle of unmodified and silane-modified samples using a drop shape analysis system DSA 10 Mk2 from Krüss Optronic GmbH (Hamburg, Germany). The sessile drop method (axisymmetric drop shape) was applied to measure the contact angles at 22°C and 45% relative humidity. A syringe with a cannula tip (internal diameter 0.5 mm) was used to deposit droplets of water or *n*-decane on the surface of the samples. Powdery samples were pressed with 150 bar to circular discs of internal diameter of 1 cm. Each sample was measured twice. Contact angles were determined by the tangent method using the analysis software DSA version 1.80.1.2 (Krüss Optronic GmbH, Hamburg, Germany).

Thermal Stability

TGA measurements of modified EVOH and nanoclay were carried out on a TGA/DSC1 from Mettler-Toledo GmbH (Gießen, Germany) equipped with the module 835 with SDTA sensor, furnace LF110 and MX5 balance. Samples were heated with a dynamic rate of 20 K min^{-1} from 25°C to 1000°C under synthetic air. 10 mg of each sample was measured in 70 µL-Al_2O_3 crucibles. Onset-temperatures of degradation were determined by the tangent method using the STARe Software 9.30 (Mettler-Toledo GmbH, Gießen, Germany).

Preparation and Characterization of Nanocomposites

EVOH nanocomposites were prepared via solution blending. The unmodified and silane-modified EVOH samples were dissolved in hexafluoro-isopropanol (HFIP). Subsequently, 5 wt % of either unmodified or silane-modified NBt were added and the solutions were treated for 30 min with a Sonotrode HD 2200 VS 70 T (Bandelin electronic, Berlin, Germany). Afterwards, a thin film was produced by spin-coating the dispersion on a microscope slide followed by evaporation of HFIP.

Electron micrographs of nanocomposites were recorded on a scanning electron microscope (SEM) Zeiss Auriga (Zeiss microscopy GmbH, Jena, Germany). Macroscopic optical properties were tested by comparing the transparency of films prepared from modified and unmodified EVOH and NBt.

RESULTS AND DISCUSSION

Structural Characterization of Silane-Modified EVOH and Silane-Modified Nanoclay

Grafting Degree of Silane-Grafted EVOH. ^{1}H-NMR experiments were performed to determine the grafting degree of silanized EVOH. The ^{1}H-NMR-spectra of pure EVOH and of a MAOM-TMOS modified EVOH (representatively for silane-modified EVOH samples) are depicted in Figure 1.

Ethylene protons of the ethylene repeating unit and the vinyl alcohol unit in EVOH appeared at 1.23 ppm (Figure 1, *C–E*). Due to stereochemical effects regarding the configuration of a vinyl alcohol unit, methine protons of EVOH showed three doublets at 3.33 ppm, 3.60 ppm, and 3.82 ppm (Figure 1, *B*). Likewise, the resonances of the hydroxyl protons showed three doublets at 4.20 ppm, 4.47 ppm, and 4.67 ppm (Figure 1, *A*).[39–41]

Additional resonances were observed by the silanization of EVOH with MAOM-TMOS. These were related to the methylene protons [Figure 1(a) at 5.97 ppm and 5.62 ppm] and methyl protons [Figure 1(d) at 1.82 ppm] of the methacryloxy-group. The chemical shift of methoxy-groups in MAOM-TMOS [Figure 1(c)] originally appeared at 3.39 ppm but vanished due to the condensation reaction. Hence, resonances of methoxy-protons were not present in the ^{1}H-NMR-spectrum of silanized EVOH. The chemical shift of the methylene protons in the Si-C***H₂***-O-bridge [Figure 1(b)] at 3.72 ppm was overlapped by the three resonances of the methine protons of EVOH (Figure 1, *B*).

As in case of MAOM-TMOS, the original resonance of methoxy-protons of GOP-TMOS at 3.49 ppm (Figure 2, ***H1***) disappeared after silanization in the corresponding ^{1}H-NMR-spectrum. Further, chemical shifts of protons in positions ***H2***, ***H3*** at 0.60 ppm and 1.57 ppm (Figure 2) were overlapped by the resonances of ethylene protons in EVOH (Figure 1*C–E*). The chemical shifts of the protons in positions ***H4*** to ***H7*** were also overlapped by the three signals of the methine protons in EVOH (Figure 2, ***H4–H7***, Figure 1, *B*)

Grafting degree of EVOH $G_{D_{EVOH}}$ was calculated from the ratio of the integrated peak intensities of the hydroxyl-group before and after modification [eq. (12), Figure 1]. Herein the chemical shift of ethylene protons in the EVOH backbone was used as

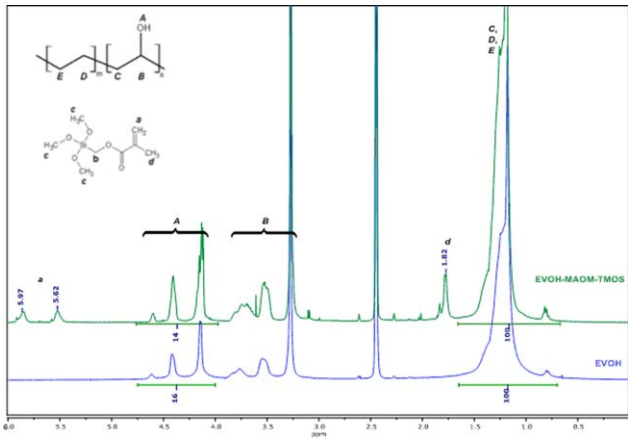

Figure 1. Comparison of ^{1}H-NMR-spectra of pure EVOH (blue line) and MAOM-TMOS modified EVOH (green line). Marking characteristic chemical shifts and peak integrals for determination of the grafting degree. [Color figure can be viewed in the online issue, which is available at wileyonlinelibrary.com.]

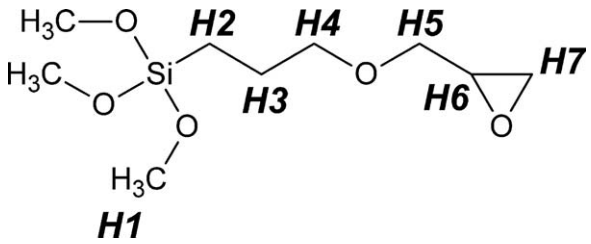

Figure 2. Chemical structure of GOP-TMOS marking positions of characteristic protons.

the reference peak to compare the chemical shifts of the hydroxyl-group before and after the silane modification.[42–47]

$$G_{D_{\mathrm{EVOH}}} = \left(1 - \frac{A_{\mathrm{after}}}{A_{\mathrm{before}}}\right) \times 100\% \qquad (12)$$

Stoichiometric compositions of EVOH and silanes were mixed in a 3-factor 2-level full factorial experimental screening design for the determination of optimum grafting conditions. The three factors varied were silane type, reaction pH and time. For modification with MAOM-TMOS grafting degrees of EVOH were in the range from 11% to 19%. GOP-TMOS-treated EVOH samples yielded a grafting from 13% to 17%. ANOVA analysis of the screening design for the EVOH-silane modification yielded the interaction between reaction time and pH as the only statistically significant effect. Whereas both time and temperature need to be integrated into the two-factor interaction model to provide for mathematically correct model hierarchy, the factor silane was definitely not statistically significant. This means that the chemical modification of EVOH under the studied reaction conditions works equally well for both silanes. The importance of the pH-reaction time interaction can be rationalized by the established fact that the relative rates of silane hydrolysis and silane condensation are very much pH dependent.[48] While the hydrolysis of alkoxy silanes is favored by lower pH, the condensation is favored by higher pH. For all further experiments with the nanoclay filler, the samples prepared at low pH (4.6) and short reaction times (6 h) were used since they displayed the highest absolute values in measured grafting degrees. Additional recordings of ^{29}Si-NMR-spectra of the EVOH samples were conducted to investigate further condensation reactions of MAOM-TMOS and GOP-TMOS. On the basis of applied silanes there was one kind of Si-nucleus to be observed in the corresponding spectra (Figure 5, T^n, $n = 0,\ldots,3$). The Si-nucleus in MAOM-TMOS and GOP-TMOS is assigned as T^n-group ($n = 0, 1, 2, 3$), since up to three Si–O–Si-bridges can be established, indicated by the superscript "n". Such T^n-groups have chemical shifts in the range of −50 ppm to −70 ppm depending on the number n.[49] Figure 3 depicts representatively for all EVOH samples the ^{29}Si-NMR-spectrum of EVOH treated with MAOM-TMOS. The sole existence of a single T^3-peak at −66.75 ppm indicated that in addition to the successful grafting to EVOH the silane molecules condensed completely.

To complement the results of NMR spectroscopy, infrared spectra were recorded of unmodified and silane-modified EVOH

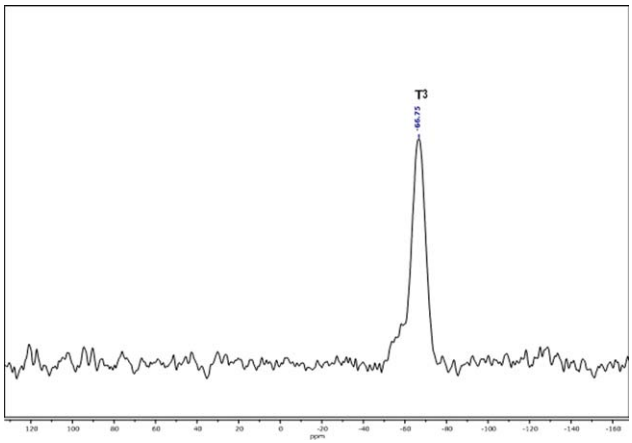

Figure 3. ^{29}Si-NMR-spectrum of EVOH treated with MAOM-TMOS representative for silanized EVOH samples. [Color figure can be viewed in the online issue, which is available at wileyonlinelibrary.com.]

(Figure 4). As seen in Figure 4, the absorbance of the stretching vibration characteristic for the hydroxyl-group $\nu(OH)$ at 3370 cm^{-1} of EVOH decreased upon silane modification. This indicates the successful grafting of silane onto the EVOH backbone for MAOM-TMOS as well as for GOP-TMOS. In case of the MAOM-TMOS modification of EVOH, the appearance of the carbonyl stretching vibration $\nu(C{=}O)$ at 1750 cm^{-1} also corroborates successful grafting of silane onto EVOH.

Silane Grafted Nanoclay. ^{29}Si-CP/MAS-NMR spectra were recorded to investigate coupling of MAOM-TMOS and GOP-TMOS to the nanoclay surface. In layered silicates so called Q^m-groups ($m = 0$, 1, 2, 3, 4) are observed, related to Si-nuclei which can form up to 4 Si–O–Si-bridges in a clay matrix (Figure 5). As a consequence of the geometry of silicates, Si-nuclei represented by Q^4-groups are located in the interior of the clay matrix, while Si-nuclei of Q^3-groups are situated on the surface or edge of a clay sheet. In dependence of the value for m, the

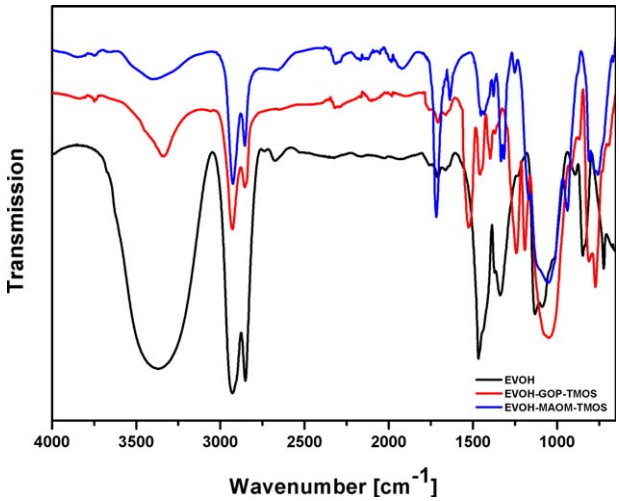

Figure 4. Infrared-spectra of unmodified and silane-modified EVOH. [Color figure can be viewed in the online issue, which is available at wileyonlinelibrary.com.]

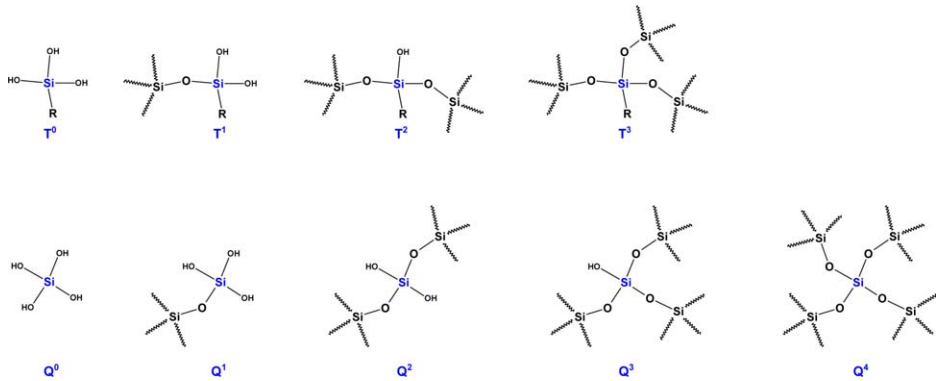

Figure 5. Differentiation between T^n- and Q^m-Si-nuclei in dependence of the number of Si–O–Si bridges. [Color figure can be viewed in the online issue, which is available at wileyonlinelibrary.com.]

corresponding ^{29}Si-resonances are shifted in the range −80 ppm to −110 ppm.[49]

Thus, potential coupling positions for silane molecules are located on the surface of the nanoclay sheets. In case of successful coupling of silanes to nanoclay surface Q^3-groups would turn into Q^4-groups resulting in a decreasing Q^3-peak. Since NBt consisted of natural bentonite it contained also aluminum atoms in the clay matrix. The additional aluminum induced overlapping of Q^3- and Q^4-peaks rendering the proof of successful coupling of silanes onto NBt surface difficult.[50] In the ^{29}Si-NMR-spectra of nanoclay samples (not shown) it was thus only possible to detect formation of T^3-groups indicating complete condensation of silane molecules. It is known from the scientific literature that the exact number of accessible hydroxyl-groups on the nanoclay surface is hard to determine for grafting reactions.[51–53] This was also found in the present study where no grafting degree could be specified for the silane modification of NBt. However, additional thermogravimetry-mass spectrometric analysis was performed on each type of modified nanoclay in order to determine whether or not organic residues were bound to the nanoclay or not. It was found that during degradation in the TGA experiment, the main volatile fragments were CO and CO_2. This indicates the degradation of an organic species and at least allows the conclusion that nanoclay surface was successfully modified by both of the applied silanes.

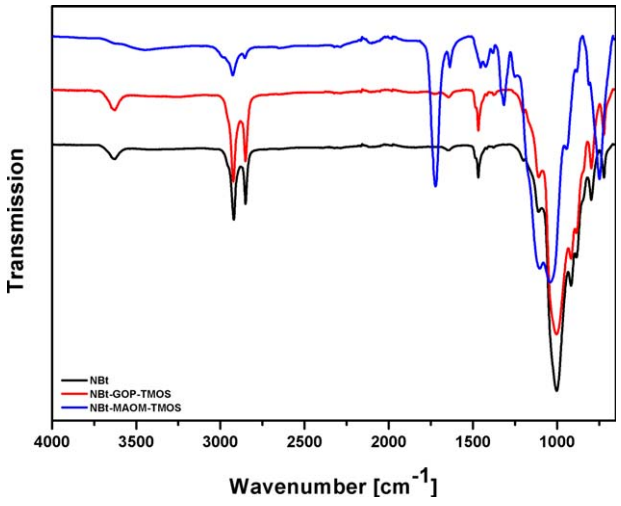

Figure 6. Infrared-spectra of unmodified and silane-modified NBt. [Color figure can be viewed in the online issue, which is available at wileyonlinelibrary.com.]

Since ^{29}Si-NMR spectroscopy turned out not to be the appropriate method to identify the attachment of silanes to the clay surface, infrared spectra were recorded of unmodified and silane-modified NBt to study the surface modification (Figure 6). Comparison of the infrared spectra of pristine NBt and GOP-TMOS modified NBt revealed no qualitative changes of the vibrational spectrum indicative for the coupling of GOP-TMOS to the clay surface. In the case of modifying NBt with MAOM-TMOS, the carbonyl stretching vibration $\nu(C{=}O)$ of the methacryloxy-group appeared at 1722 cm^{-1} corroborating sufficient surface modification of the clay surface.

Interfacial compatibility can greatly assist intercalation and exfoliation in case of layered silicates.[54,55] Therefore, X-ray diffraction measurements (XRD) were conducted to investigate the effect of silane-modification on the inter-layer distance of nanoclay samples. As seen in Figure 7, pristine NBt yielded a basal spacing between 26 Å and 30 Å. This can be explained by the surfactant-modification with distearyl-dimethyl-ammonium chloride of the nanoclay by the manufacturer. The applied surfactant molecule with its chain length of 18 carbon atoms is very flexible, so that the inter-layer distance of the nanoclay can vary in a broad range. This wide distribution of inter-layer distances causes the plateau observed for the pristine NBt (Figure 7, black line).

Upon modification of NBt with GOP-TMOS, the long-chained surfactant molecule is replaced by GOP-TMOS. As a result, the number of possible inter-layer distances is reduced and a shift of the average interlayer distance to approximately 27 Å is observed (Figure 7, red line). A similar effect is observed with MAOM-TMOS. However, in this case the modification led to a significantly increased inter-layer distance (38 Å, see Figure 7, blue line).

These observations are in good agreement with the literature,[55] where nanoclay modification by a tri-functional silane also caused an increase in the inter-layer distance in nanoclay,

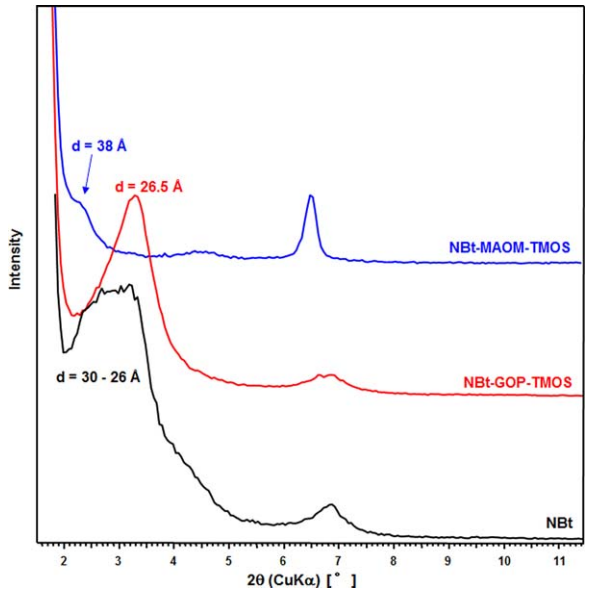

Figure 7. XRD patterns of unmodified NBt (black line), NBt-GOP-TMOS (redline), and NBt-MAOM-TMOS (blue line). [Color figure can be viewed in the online issue, which is available at wileyonlinelibrary.com.]

whereas modification with a mono-functional silane did not. The authors explained their findings with a polycondensation reaction of the used tri-functional silane at the edge zones of the platelets which was not possible in the case of the mono-functional silane.

In agreement with these earlier observations, in case of the silanes used in the present study, the increase in interlayer distance observed with MAOM-TMOS can also be explained with the formation of such polysiloxanes. GOP-TMOS in contrast, although carrying a tri-functional moiety as well can alternatively also react as a mono-functional molecule with its glycidoxy group. Considering the relative reactivities of the glycidoxy and the trimethoxysilyl functionalities, it is assumed that the attachment of the silane to the nanoclay with the mono-functional part of the molecule should more preferably occur than attachment with the trimethoxysilyl-end. This would provide an explanation for the observation that GOP-TMOS does not significantly increase the inter-layer distance of NBt. The reason why GOP-TMOS leads to a smaller interlayer distance than does MAOM-TMOS may be related to the relative orientations of the tri-functional groups of the silane molecules after nanoclay modification as follows: according to Herrera et al.,[55] silane modifiers bind to the nanoclay platelets preferably at the edges of the single layers rather than at sites located within the interlaminate space. Modification of the nanoclay with a multi-functional silane ultimately produces a polycondensation product (a polysiloxane) that pushes the clay-sheets apart. If the tri-functional silane is directly linked to the nanoclay with its hydrolyzed tri-methoxysilyl head, polycondensation is forced to take place in close proximity to the platelets and hence, their inter-layer distance is increased. Moreover, polysiloxane bridges may be formed between the platelets. If, however, as in the case of GOP-TMOS, the silane is linked to the platelet edge via the opposite end of the molecule, i.e., its glycidoxy group, its tri-functional end points outwards and the resulting polycondensates are not as close to the single layers, resulting in a reduced ability to push apart and cross-link the layers.

Table III. Specific Surface Areas and Total Pore Volumes Determined by the BET- and BJH Methods of Pristine NBt, MAOM-TMOS, and GOP-TMOS-Modified NBt

Sample	A_{BET}[a] ($m^2\ g^{-1}$)	V_{Pore}[b] ($cm^3\ g^{-1}$)
NBt	11.3	0.12
NBt-GOP-TMOS	4.5	0.04
NBt-MAOM-TMOS	2.3	0.03

[a] Specific surface area determined by the Brunauer-Emmett-Teller (BET) method.
[b] Total pore volume determined by the Barrett-Joyner-Halenda (BJH) method.

As an observable effect of such silane modification, the inner surface of the nanoclay would be blocked by the organic molecules grafted.[56] Hence, the specific surface area of the modified nanoclays would appear to be reduced when assessed by adsorption measurement methods like the Brunauer-Emmett-Teller (BET) or the BJH methods because of the screening effect of the silanes. This blocking effect should be more pronounced in the case of MAOM-TMOS due to the spatially more restricted siloxane polycondensation.

To test this hypothesis, BET and BJH measurements were performed on the nanoclays. The values of the BET specific surface areas and of the BJH values for the total pore volumes of the modified nanoclays samples were indeed much lower than the value for the pristine nanoclay (Table III). Moreover, the MAOM-TMOS modified nanoclay displayed a smaller specific surface area and a smaller total pore volume than the GOP-TMOS modified one. The pore size distribution indicated formation of a porous structure upon GOP-TMOS modification whereas the MAOM-TMOS modified sample displayed practically no porosity at all. These findings corroborate the more pronounced screening effect of MAOM-TMOS as would be expected in the case of an inward orientation of the tri-functional group.

Surface Properties and Thermal Stability of EVOH and Nanoclay

Contact angle measurements were conducted to assess the surface properties of unmodified and silane-modified samples. However, the obtained values were not conclusive due to high porosity of the samples (circular discs, pressed at 150 bar).

As compared to contact angle, IGC allows to measure porous or powdery samples. Moreover, the interfacial properties are determined more directly since here the surface energy is investigated on a molecular level by the interaction of a probe molecule with the solid. Hence, IGC was applied to characterize the surface properties of unmodified and modified EVOH and nanoclay.

A series of *n*-alkanes were injected to calculate the dispersive surface energy following the approach of Schultz.[30] Further application of polar probes (chloroform, 1,4-dioxane,) during IGC experiments was used to determine Lewis acid-base

Table IV. Dispersive, Specific Surface Energies, Lewis Acid–Base Properties, and Degradation Onset Temperatures of EVOH and Nanoclay Samples

Sample	$\gamma_S^D\,[mJ\cdot m^{-2}]$	$\Delta G^{sp}\,[mJ\cdot m^{-2}]$		$\frac{\Delta G^{sp}(Dioxane)}{\Delta G^{sp}(Chloroform)}$	T_{on} [°C]
		Chloroform	1,4-Dioxane		
EVOH	42.14±0.45	11.88	42.68	3.59	301
NBt	41.99±0.44	23.11	80.99	3.50	207
EVOH-MAOM-TMOS	46.22±0.54	23.50	63.83	2.72	351
NBt-MAOM-TMOS	47.40±1.16	24.16	73.50	3.04	291
EVOH-GOP-TMOS	49.48±0.25	30.99	71.84	2.32	341
NBt-GOP-TMOS	48.22±0.36	24.50	73.76	3.01	243

γ_S^D: dispersive surface energy; ΔG^{sp}: specific surface energy; T_{on}: degradation onset temperature.

properties of the unmodified and modified samples. The calculated surface properties and thermal properties of EVOH and nanoclay are listed in Table IV. Surface and thermal properties of modified EVOH and nanoclay were independent from either reaction conditions or silane concentrations.

As seen in Table IV untreated EVOH and NBt had similar dispersive surface energies of about 42 mJ m^{-2}. Likewise, both samples displayed relatively high Lewis-acidic surfaces of approximately 3.5. In case of modification of EVOH and NBt with MAOM-TMOS, dispersive surface energies increased in a similar way to 46–47 mJ m^{-2}. Further, Lewis-acidity decreased significantly, which can be explained by a decreasing number of free hydroxyl-groups in EVOH as well as in NBt. This observation is in good agreement with a successful grafting result, as indicated by NMR-, TGA/mass spectrometric-measurements or infrared spectra. Similar adaptation of the surface properties was also observed modifying EVOH and NBt with GOP-TMOS (Table IV).

Modification of EVOH and NBt with different silanes yielded a significantly increased thermal stability of both the modified EVOH and the modified nanoclay as was determined by TGA in terms of the onset temperature, T_{on} of thermal degradation (Table IV).

Silanization of EVOH with MAOM-TMOS yielded a much more robust modification of the polymer ($T_{on} = 351$°C) than the GOP-TMOS treatment ($T_{on} = 341$°C) or no treatment (pristine EVOH, $T_{on} = 301$°C) (Figure 8, 9). This can be explained by the type of linkage established between silanes and EVOH. Using MAOM-TMOS as the modifying agent, only Si–O–C-bridges can be formed between silane and polymer. In case of GOP-TMOS, however, it is also possible to form C–O–C-bridges. Since a C–O–C-bridge is less stable (716 kJ mol^{-1}) than a Si-O-C-bridge (802 kJ mol^{-1}), modification of EVOH with GOP-TMOS would be expected to yield a less stable product than does modification of EVOH with MAOM-TMOS.[57]

In case of the nanoclay, T_{on} of pristine NBt (207°C) was increased to 291°C (NBt-MAOM-TMOS) and 243°C (NBt-GOP-TMOS) by the modification with MAOM-TMOS and GOP-TMOS, respectively. This can be explained analogously: MAOM-TMOS can only be attached to the nanoclay surface by Si–O–Si-bridges, whereas GOP-TMOS can also form Si–O–C-bridges. Here a Si–O–Si-bridge (888 kJ mol^{-1}) is more stable than a Si–O–C-bridge, so that the MAOM-TMOS modified NBt is thermally more stable than the GOP-TMOS-modified NBt.[57] These results are in good agreement with earlier findings of Geyer et al.[58] that MAOM-TMOS treatment of nanoclay leads to a thermally more stable modification than a treatment by GOP-TMOS. Enhanced thermal stability is of crucial

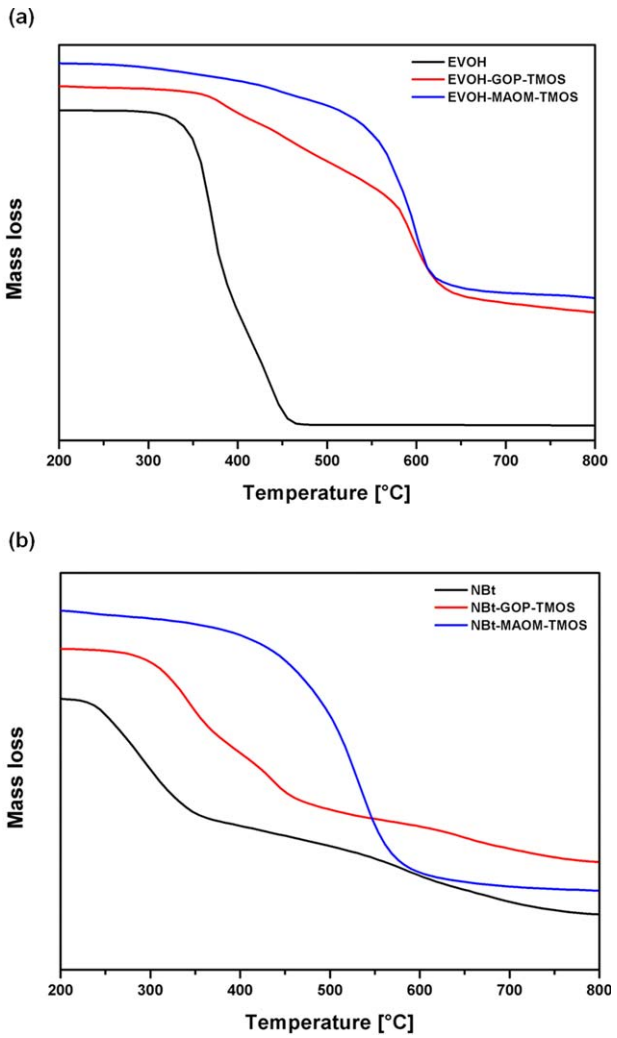

Figure 8. TGA-traces of unmodified and silane-modified EVOH (a) and NBt (b). [Color figure can be viewed in the online issue, which is available at wileyonlinelibrary.com.]

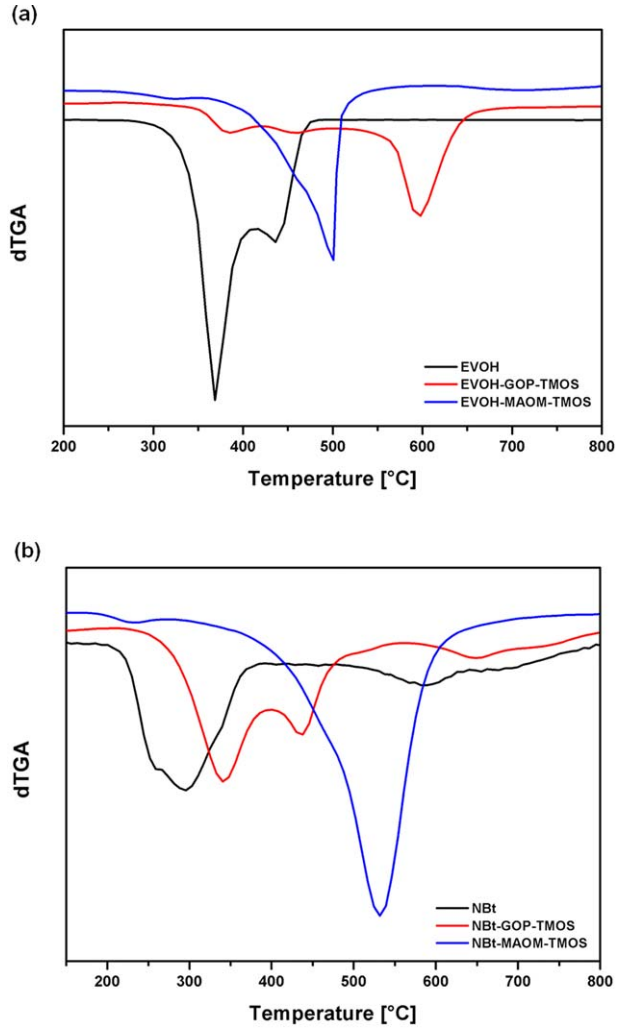

Figure 9. dTGA-traces of unmodified and silane-modified EVOH (a) and NBt (b). [Color figure can be viewed in the online issue, which is available at wileyonlinelibrary.com.]

importance regarding further processing of such materials. Processing of polymers and nanoclays in general entails exposition to elevated temperatures. Thus, thermal stability is necessary in order to maintain silane modification and thereby, compatibility between the blend components during processing.

Morphological Characterization of Nanocomposites

Scanning electron microscopy was applied to investigate the effect of surface modification of both EVOH and nanoclay on the dispersibility of nanoclay particles in the polymer matrix. The following nanocomposites were prepared and studied with SEM (Figure 10): EVOH, unmodified/NBt, MAOM-TMOS modified [Figure 10(a)]; EVOH, unmodified/NBt, unmodified [Figure 10(b)]; EVOH, MAOM-TMOS modified/NBt, MAOM-TMOS modified [Figure 10(c)], EVOH, GOP-TMOS modified/NBt, GOP-TMOS modified [Figure 10(d)].

The sample shown in Figure 10(a) illustrates an incompatible mixture of the components: combination of unmodified EVOH with MAOM-TMOS modified NBt led to nanoclay agglomerates with a particle size of approximately 1 micrometer dispersed in the polymer matrix. As evident from the insert in Figure 10(a), even larger agglomerates in the order of magnitude of several micrometers were present. Further, dispersion of these particles in the polymer was not very homogeneous.

The nanocomposite where neither EVOH nor NBt was silane-modified [Figure 10(b)] yielded a reduction in clay particle size associated with a more homogeneous dispersion of clay particles.

Where both EVOH and NBt were modified with silane a significantly improved homogeneity of nanoclay particle dispersion in the polymer matrix was the result [Figure 10(c, d)], no matter whether MAOM-TMOS [Figure 10(c)] or GOP-TMOS [Figure 10(d)] were applied. All particles were of nanoscale size [Figure 10(c, d), bright small spots] and no larger agglomerates were observed. These results show that for good compatibility it is not sufficient that the blend components possess similar values for their surface energies, but that it is also required that they display similar surface chemistry in order to produce a homogeneous nanocomposite. The improved compatibility between EVOH and NBt is also evident when macroscopic properties are considered. Figure 11 shows photographs of one compatible [EVOH, MAOM-TMOS modified/NBt, MAOM-TMOS modified, Figure 11(a)] and one incompatible [EVOH, unmodified/NBt, MAOM-TMOS modified, Figure 11(b)] nanocomposite film. It is seen that when both components of the nanocomposite were chemically modified by MAOM-TMOS, the brilliance of the image covered by the transparent nanocomposite sheet became much better. Brilliant optical transparency was only achieved when the nanoscaled particles were homogeneously dispersed in the polymer matrix.

CONCLUSION

Ethylene vinyl alcohol and the nanoclay NBt were modified with different silanes, MAOM-TMOS, and GOP-TMOS. Starting materials as well as grafted species were characterized by NMR-spectroscopy, infrared spectroscopy, IGC, contact angle measurements, and thermogravimetry. ^{1}H-NMR-measurements proved for every silane successful grafting onto EVOH surface. In addition, ^{29}Si-NMR-measurements revealed complete condensation of the applied silanes. Further, infrared spectra of unmodified and modified EVOH samples corroborated successful grafting of silanes onto EVOH surface. In case of NBt it was not possible to prove covalent coupling of silanes to silicate surface by ^{29}Si-NMR-spectroscopy. This difficulty was attributed to the nature of the nanoclay. Additional aluminum atoms in the silicate matrix rendered differentiation between Si-atoms on the clay sheet surface (possible coupling positions for silane molecules) and Si-atoms within the clay matrix impossible. Again, ^{29}Si-NMR-spectra proved solely complete condensation of applied silanes. In contrast to the infrared spectra of the EVOH samples, only the infrared spectrum of MAOM-TMOS modified NBt corroborated sufficient surface grafting of the nanoclay. Thus, additional thermogravimetry-mass spectrometric analysis and a decreasing Lewis-acidity of nanoclay supported successful modification of NBt by silane treatment. XRD-measurements of silane-modified

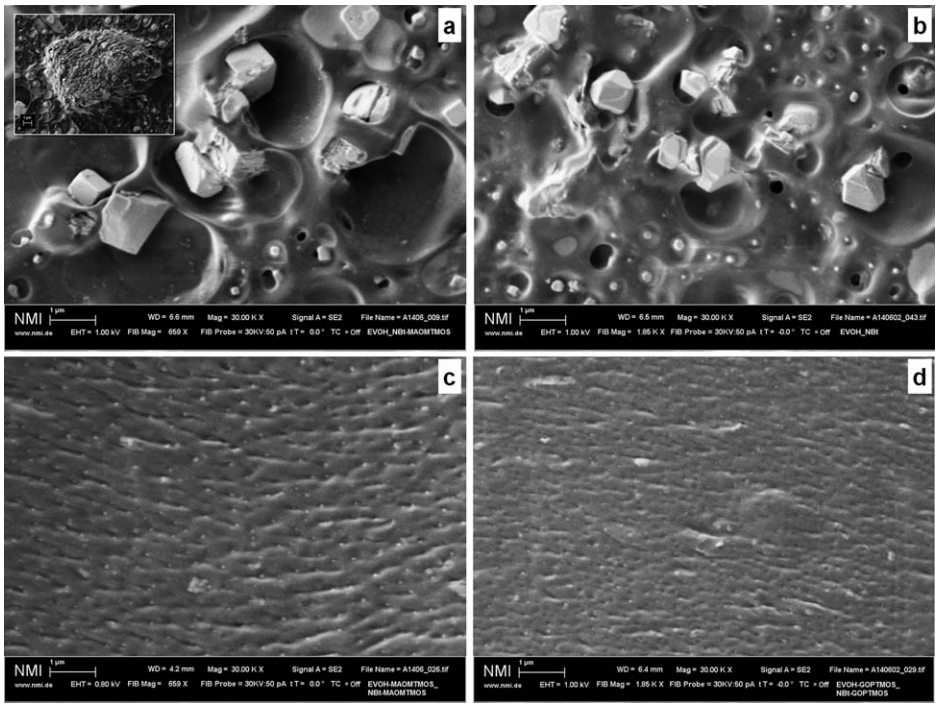

Figure 10. Nanocomposite SEM micrographs of (a) EVOH and MAOM-TMOS modified NBt, (b) unmodified EVOH and NBt, (c) MAOM-TMOS modified EVOH and MAOM-TMOS modified NBt, (d) GOP-TMOS modified EVOH and GOP-TMOS-modified NBt.

NBt showed that MAOM-TMOS modification yielded an increased inter-layer distance compared to pristine NBt. Characterization of surface properties represented by the dispersive surface energies showed good compatibility of modified EVOH and the nanoclay to each other. Determination of degradation onset temperatures revealed an enhanced thermal stability of modified EVOH and nanoclay in comparison to unmodified EVOH or NBt. Improved compatibility and enhanced thermal stability are important features to facilitate further processing. Finally, as a result of silane-modification, improved compatibility of EVOH and NBt yielded a homogeneous dispersion of nanoscaled clay particles in the polymer matrix to give films of much improved transparency. The proposed method should be applicable in principle to all polymer matrix systems that bear potential coupling positions for silanes or are susceptible to silane grafting.

Figure 11. Nanocomposite films of (a) EVOH-MAOM-TMOS and NBt-MAOM-TMOS and (b) EVOH and NBt-MAOM-TMOS.

ACKNOWLEDGMENTS

The authors would like to thank the project management Jülich, Forschungszentrum Jülich (project number: 17 N18 10) for supporting the project in financial terms, Prof. Dr. Klaus Albert and his group of the University of Tübingen (Germany) for performing the ^{1}H-NMR-measurements, Prof. Dr. Hermann A. Mayer and his group at the University of Tübingen (Germany) for conducting ^{29}Si-solid-state NMR experiments, Dr. Volker Hagen (Rubokat GmbH, Bochum, Germany) for conducting the additional mass spectrometric and nitrogen adsorption measurements, Dr. Christoph Berthold (University of Tübingen, Germany) for conducting the XRD-measurements, and Clementine Warres (The Natural and Medical Sciences Institute NMI, Reutlingen) for recording the electron micrographs.

REFERENCES

1. Kit, K. M.; Schultz, J. M.; Gohil, R. M. *Polym. Eng. Sci.* **1995**, *35*, 680.
2. George, E. R.; Sullivan, T. M.; Park, E. H. *Polym. Eng. Sci.* **1994**, *34*, 17.
3. Sadik, T.; Massardier, V.; Becquart, F.; Taha, M. *J. Appl. Polym. Sci.* **2013**, *127*, 1148.

4. Aoki, Y.; Li, L.; Amari, T.; Nishimura, K; Arashiro, Y. *Macromolecules* **1999**, *32*, 1923.
5. Landry, C. J. T.; Massa, D. J.; Teegarden, D. M.; Landry M. R.; Henrichs, P. M.; Colby, R. H.; Long T. E. *Macromolecules* **1993**, *26*, 6294.
6. Po, R.; Occhiello, E.; Giannotta, G.; Pelosini, L.; Abis, L. *Polym. Advan. Technol.* **1995**, *7*, 365.
7. Rwei, S. P. *Polym. Eng. Sci.* **1999**, *39*, 2475.
8. Guo, M.; Brittain, W. J. *Macromolecules* **1998**, *31*, 7166.
9. Zhang, Q.; Ma, X.; Wang, Y.; Kou, K. *J. Phys. Chem. B* **2009**, *113*, 11898.
10. Artzi, N.; Narkis, M.; Siegmann, A. *J. Polym. Sci. Pol. Phys.* **2005**, *43*, 1931.
11. Artzi, N.; Tzur, A.; Narkis, M.; Siegmann, A. *Polym. Compos.* **2005**, *26*, 343.
12. Manias, E.; Touny, A.; Wu, L.; Strawhecker, K.; Lu, B. Chung, T. C. *Chem. Mater.* **2001**, *13*, 3516.
13. Chiu, C.-W.; Cheng, W.-T.; Wang, Y.-P.; Lin, J.-J. *Ind. Eng. Chem. Res.* **2007**, *46*, 7384.
14. Beyer, F. L., Beck Tan , N. C., Dasgupta, A., Galvin, M. E. *Chem. Mater.* **2002**, *14*, 2983.
15. Kimura, T., Itoh, D., Okazaki, N., Kaneda, M., Sakamoto, Y., Terasaki, O., Sugahara,Y., Kuroda, K. *Langmuir* **2000**, *16*, 7624.
16. Kurian, M., Dasgupta, A., Galvin, M. E., Ziegler, C. R., Beyer, F. L. *Macromolecules* **2006**, *39*, 1864.
17. Zerda, A. S., Caskey, T. C., Lesser, A. J. *Macromolecules* **2003**, *36*, 1603.
18. Touhtouh, S.; Becquart, F.; Pillon, C.; Taha, M. *Polymers* **2011**, *3*, 1734.
19. Pesneau, I.; Llauro, M. F.; Grégoire, M.; Michel, A. *J. Appl. Polym. Sci.* **1997**, *65*, 2457.
20. Artzi, N.; Narkis, M.; Siegmann, A. *Polym. Eng. Sci.* **2004**, *44*, 1019.
21. Brocorens, P.; Benali, S.; Broekaert, C.; Monteverde, F.; Miltner, H. E.; Van Mele, B.; Alexandre, M.; Dubois, P.; Lazzaroni, R. *Langmuir* **2008**, *24*, 2072.
22. Abdelmouleh, M.; Boufi, S.; Salah, A.; Belgacem, M. N.; Gandini, A. *Langmuir* **2002**, *18*, 3203.
23. Alvi, M. U.; Zulfiqar, S.; Yavuz, C. T.; Kweon, H.-S.; Sarwar, M. I. *Ind. Eng. Chem. Res.* **2013**, *52*, 6908.
24. Muppalla, R.; Jewrajka, S. K. *Ind. Eng. Chem. Res.* **2012**, *51*, 15942.
25. Mittal KL, Ed. Acid-Base Interactions: Relevance to Adhesion Science and Technology; VSP BV: Utrecht, **2000**.
26. Osman, M. A.; Mittal, V.; Morbidelli, M.; Suter, U. W. *Macromolecules* **2004**, *37*, 7250.
27. Hu, D. S.-G.; Tsai, C.-E. *J. Appl. Polym. Sci.* **1996**, *59*, 1809.
28. Kim, D.-K.; Lee, S.-B.; Doh, K.-S.; Nam, Y.-W. *J. Appl. Polym. Sci.* **1999**, *74*, 2029.
29. Der-Jang, L.; Bing-Yaun, S. *Angew. Macromol. Chem.* **1993**, *212*, 77.
30. Schultz, J.; Lavielle, L. In Inverse Gas Chromatography: Characterization of Polymers and Other Materials; Lloyd, D. R.; Ward, T. C.; Schreiber, H. P.; Pizaña, C. C., Eds.; American Chemical Society: Washington, D.C., **1989**; Vol. 391, Chapter 14, p 185.
31. Shi, B.; Wang, Y., Jia, L. *J. Chromatogr. A* **2011**, *1218*, 860.
32. Schultz, J.; Lavielle, L.; Martin, C. *J. Adhes.* **1987**, *23*, 45.
33. Dorris, G. M.; Gray, D.G. *J. Colloid Interf. Sci.* **1980**, *77*, 353.
34. Fowkes, F. M. *Ind. Eng. Chem.* **1964**, *56*, 40.
35. Schultz, J.; Lavielle, L.; Martin, C. *J. Chim. Phys.* **1987**, *84*, 231.
36. Lara, J.; Schreiber, H. P. *J. Coat. Technol.* **1991**, *63*, 81.
37. Liu, F. P.; Rials, T. G.; Simonsen, J. *Langmuir* **1998**, *14*, 536.
38. Kamdem, D. P.; Bose, S. K.; Luner, P. *Langmuir* **1993**, *9*, 3039.
39. Wu, T. K. *J. Polym. Sci.* **1976**, *14*, 343.
40. Zhang, Q. J.; Chen, Q. *Chem. J. Chinese U.* **2003**, *24*, 728.
41. Fernández, M. J.; Fernández, M. D. *Polymer* **2005**, *46*, 1473.
42. Cerrada, M. L.; Sánchez-Chaves, M.; Ruiz, C.; Fernández-García, M. *Biomacromolecules* **2009**, *10*, 1828.
43. Liu, B.; Xue, Z.; Liu, L.; Zhang, L.; Liu, F. *J. Appl. Polym. Sci.* **2006**, *102*, 227.
44. Marconi, W.; Cordelli, S.; Napoli, A.; Piozzi, A. *Macromol. Chem. Phys.* **1999**, *200*, 1191.
45. Bruzaud, S. Levesque, G. *Macromol. Chem. Phys.* **2000**, *201*, 1758.
46. Pesneau, I.; Grégoire, M.; Michel, A. *J. Appl. Polym. Sci.* **2001**, *79*, 1556.
47. Giménez, V.; Mantecón, A.; Ronda, J. C.; Cádiz, V. *J. Appl. Polym. Sci.* **1997**, *65*, 1643.
48. Rösch, L.; John, P.; Reitmeier, R. In Silicon Compounds, Organic Ullmann's Encyclopedia of Industrial Chemistry; Wiley: New York, **2005**, Band 24, p 34.
49. Lindner, E.; Schneller, T.; Auer, F.; Mayer, H. A. *Angew. Chem.* **1999**, *111*, 2288.
50. Lippmaa, E.; Mägi, M.; Samoson, A.; Engelhardt, G.; Grimmer, A.-R. *J. Am. Chem. Soc.* **1980**, *102*, 4889.
51. Hanke, W. Z. *anorg allg. Chem.* **1973**, *395*, 191.
52. Duc, M.; Gaboriaud, F.; Thomas, F. *J. Colloid Interf. Sci.* **2005**, *289*, 139.
53. Warkentin, B. P. *Kolloid. Z.* **1957**, *153*, 44.
54. Boo, W. J.; Sun, L.; Liu, J.; Clearfield, A.; Sue, H.-J. *J. Phys. Chem. C*, **2007**, *111*, 10377.
55. Herrera, N.; Letoffe, J.-M.; Putaux, J.-L.; David, L.; Bourgeat-Lami, E. *Langmuir*, **2004**, *20*, 1564.
56. Nguyen, P. T. M.; Fan, C.; Do, D. D.; Nicholson, D. *J. Phys. Chem. C* **2013**, *117*, 5475.
57. Riedel, E. In Anorganische Chemie; Walter de Gruyter: Berlin, New York, **2004**; Chapter *2*, p 119.
58. Geyer, B.; Hundshammer, T.; Röhner, S.; Lorenz, G.; Kandelbauer, A. *Appl. Clay Sci. submitted.*